Ammonia snow-lines and ammonium salts desorption ⋆

F. Kruczkiewicz[1,2,3], J. Vitorino[2], E. Congiu[2], P. Theulé[1], and F. Dulieu[2]

[1] Aix Marseille Univ, CNRS, CNES, LAM, Marseille, France
  e-mail: franciele.kruczkiewicz@lam.fr
[2] CY Cergy Paris Université, Observatoire de Paris, PSL University, Sorbonne Université, CNRS, LERMA, F-95000, Cergy, France
[3] Max-Planck-Institut für extraterrestrische Physik, Gießenbachstraße 1, Garching, 85748, Germany

ABSTRACT

Context. The nitrogen reservoir in planetary systems is a long standing problem. Part of the N-bearing molecules is probably incorporated into the ice bulk during the cold phases of the stellar evolution, and may be gradually released into the gas phase when the ice is heated, such as in active comets. The chemical nature of the N-reservoir should greatly influence how, when and in what form N returns to the gas phase, or is incorporated into the refractory material forming planetary bodies.
Aims. We present the study the thermal desorption of two ammonium salts: ammonium formate and ammonium acetate from a gold surface and from a water ice substrate.
Methods. Temperature-programmed desorption experiments and Fourier transform infrared reflection spectroscopy were conducted to investigate the desorption behavior of ammonium salts.
Results. Ammonium salts are semi-volatile species releasing neutral species as major components upon desorption, that is ammonia and the corresponding organic acid ($HCOOH$ and CH_3COOH), at temperatures higher than the temperature of thermal desorption of water ice. Their desorption follows a first-order Wigner-Polanyi law. We find the first order kinetic parameters A = $7.7 \pm 0.6 \times 10^{15}$ s^{-1} and E_{bind} = 68.9 ± 0.1 kJ mol^{-1} for ammonium formate and A = $3.0 \pm 0.4 \times 10^{20}$ s^{-1} and E_{bind} = 83.0 ± 0.2 kJ mol^{-1} for ammonium acetate. The presence of a water ice substrate does not influence the desorption kinetics. Ammonia molecules locked in salts desorb as neutral molecules at temperatures much higher than previously expected that are usually attributed to refractory materials.
Conclusions. Ammonia snow-line has a smaller radius than the water snow-line. As a result, the NH_3/H_2O ratio content in solar system bodies can be a hint as to where they formed and subsequently migrated.

Key words. astrochemistry – molecular processes – methods: laboratory: solid state – ISM: molecules – Protoplanetary disks – Comets: general

1. Introduction

The abundance of nitrogen, the fifth most abundant element in the Universe, has always been a matter of debate (Maiolino & Mannucci 2019), both in the extra-galactic interstellar medium (ISM) and in the local ISM, because nitrogen has both a primary and a secondary nucleosynthetic contribution (Vila-Costas & Edmunds 1993), and because nitrogen has a significant depletion factor of 0.89 (Savage & Sembach 1996) indicating that a fraction of nitrogen has been incorporated into dust grains (mainly as titanium nitride, TiN). In the solar system as well, the N abundance is among the more uncertain elemental abundances (Lodders 2010); it has been estimated to be 7.24×10^{-5} with respect to hydrogen (Caffau et al. 2009; Grevesse et al. 2010). Nitrogen can have several carriers, depending on the phase of the ISM. In the diffuse ISM, nitrogen is mostly atomic, neutral or ionized; the column densities derived from VUV and UV absorption lines of molecular nitrogen (Knauth et al. 2004) is several orders of magnitude lower than that of atomic nitrogen (Nieva & Przybilla 2012). In dense clouds, although neutral nitrogen (NI) and molecular nitrogen (N_2) are not observable directly, indirect observations using diazenylium (N_2H^+) (Maret et al. 2006) lead to

the conclusion that atomic nitrogen is the dominant reservoir of nitrogen.

Other N-bearing molecules such as NO, CN, NS and NH diatomic radicals, or NH_3, HCN, HNCO, HNC and N_2H^+ are observed with variable abundances in different sources (Omont 2007), NH_3 being the most abundant of the gas-phase carrier at a typical abundance of few 10^{-8} with respect to molecular hydrogen. In pre-stellar cores it is likely that nitrogen is incorporated into the dust grain icy mantles. A recent study by Punanova et al. (2018) illustrates this specific property and demonstrates how N-bearing molecules can map the densest parts of star-forming regions such as filaments in the Taurus molecular cloud. The hyper-fine structure of ortho-NH_3 ($1_0 - 0_0$) has been resolved for the first time in space (Caselli et al. 2017) by observing a dark molecular cloud, confirming previous estimates of dynamics and abundances. The chemical model developed underestimates the abundance of NH_3 towards the center of the nucleus by more than an order of magnitude and overestimates its abundance by about two orders of magnitude in the outer regions (Hily-Blant et al. 2010). The Spitzer ice survey showed that in star-forming regions the most abundant N-bearing ices are NH_3, NH_4^+ and OCN^-, with typical (but with large uncertainties) abundances of about 4×10^{-6}, 4×10^{-6} and 4×10^{-7} with respect to hydrogen nuclei, respectively (Boogert et al. 2015), HCN being undetected in interstellar ices. However, these three main N-carriers only account for about 10% of the overall nitrogen elemental bud-

get (Öberg et al. 2011). The missing N may be partially in the form of N_2, but the latter is almost undetectable (Boogert et al. 2015). In Young Stellar Objects and outflows, where the ice is sublimated by radiative or shock heating (Riaz et al. 2018; Tafalla et al. 2010), N-bearing molecules abundances increase but still cannot account for the initial atomic abundances. In the solar system, observations by the Rosetta mission have shown that for 67/P Churyumov-Gerasimenko, like for 1P/Halley before, cometary ices are depleted in nitrogen (Filacchione et al. 2019). The COSIMA instrument on board measured an average N/C of 0.035 ± 0.011, which is similar to the ratio found in the insoluble organic matter extracted from carbonaceous chondrite meteorites and in most micrometeorites and interplanetary dust particles (Fray et al. 2017). Comparing this ratio with the N/C value of 0.29 ± 0.12 in the solar system (Lodders 2010), we see that almost 90% of the nitrogen is missing. Recently, one of the missing reservoirs of nitrogen may have been found in comets, as the 3.2 μm absorption band is likely to be due to ammonium salts (Altwegg et al. 2020; Poch et al. 2020), with the spectrum of comet 67/P having the same shape of a laboratory spectrum of ammonium formate mixed with pyrhotite grains. Ammonium salts are semi-volatile materials that desorb at higher temperatures than the more volatile NH_3 and H_2O (Viti et al. 2004), which explains why they may have been missed by the COSIMA instrument. The temperature dependence of the solid to gas phase abundance ratio of each one of the reservoirs is fundamental to address the overall N budget. The solid phase abundance of each carrier is more easily quantified after its sublimation.

Indeed, NH_3 is central in ice chemistry (Theulé et al. 2013), as it bears the lone pair of the N atom that favors the nucleophilic addition reaction with CO_2 giving ammonium carbamate $NH_4^+NH_2COO^-$ and carbamic acid NH_2COOH (Bossa et al. 2008; Noble et al. 2014; Potapov et al. 2019), and it acts as the base in acid-base reactions with HNCO (Mispelaer et al. 2012), HCN (Noble et al. 2013), HCOOH (Bergner et al. 2016) and HCl, which gives the ammonium cyanate $NH_4^+OCN^-$, ammonium cyanide $NH_4^+CN^-$, ammonium formate $NH_4^+HCOO^-$ and ammonium chloride $NH_4^+Cl^-$ salts, respectively.

The NH_3/NH_4^+ hydride is an important tracer of the chemical evolution of the solar system, as it is detected in the proto-solar nebula, in the solar system bodies and in planetary atmospheres (Caselli & Ceccarelli 2012). This is why understanding how, and in which chemical form, it travels from the primitive molecular cloud until it is incorporated in other bodies is a key question toward understanding the complex history of the solar system formation.

Determination of the nitrogen $^{14}N/^{15}N$ or the hydrogen H/D isotopic ratios in different bodies of the solar system provides important information regarding the solar system's origin (Caselli & Ceccarelli 2012). The $^{14}N/^{15}N$ ratio varies greatly from body to body in the solar system (Hily-Blant et al. 2013): from an initial value of 441 (without corrections due to cosmic evolution) in the Solar nebula (Marty 2012), the Earth atmosphere, with a value of 272 (Marty 2012), and the solar system primitive objects, with a value of 140 in comets for all N-bearing species (HCN, CN, NH_2) (Rousselot et al. 2014) and values from 5 to 3000 in meteorites (Bonal et al. 2010) enriched in ^{15}N. Similarly, the D/H ratio can vary significantly in different objects in the solar system, from carbonaceous chondrites to comets or planetary moons (Alexander et al. 2012), and imposes constraints on the extent of their pre-solar heritage. The D/H exchange in ice is dominated by water, by its crystallization, and

is more efficient for N-bearing and O-bearing molecules rather than for C-bearing molecules (Faure et al. 2015a,b).

To make these observations meaningful, it is important to retrace the journey of the main N-carriers from the pre-solar nebula (a cold, radiation rich environment, favoring isotopic fractionation) to the solar system bodies. Although NH_3 and NH_4^+ are the main observed carriers in ice, they account for less than 10 % of the overall nitrogen elemental budget (Öberg et al. 2011); HCN or N_2 are not detected in ices (Boogert et al. 2015). While NH_3 is a volatile species (it desorbs before or with water), NH_4^+ is a refractory species, which has been detected in cometary spectra after the water ice has sublimated (Altwegg et al. 2020; Poch et al. 2020). Actually, the incorporation of nitrogen in the (acid) soluble or insoluble matter of chondrites, depends on the amount and form of N-bearing molecules inherited from the proto-solar nebula ice (Alexander et al. 2017), and the insoluble organic matter may be an important source of Earth's volatile species.

This is why reliable modeling of disk chemistry is under development (Walsh et al. 2014; Visser et al. 2018; D'Angelo et al. 2019), with the gas/surface exchange, through accretion and desorption, being an important part of the modeling. Although such a complete modeling is clearly out of the scope of this paper, we want to show how different treatments of the ammonia desorption can lead to different conclusions.

In its ammonium form, nitrogen is more refractory (Gálvez et al. 2010) and can be stored on grains in the inner side of the snow-line, which corresponds to the water ice mantle desorption. In the form of ammonium, the amount of nitrogen that can be incorporated into the planetesimals and later into primitive planetary atmospheres depends on its desorption mechanisms and is still an open question. Because of the temperature gradient in the protoplanetary disk, because of the migration of protoplanets in the disk and because this history can be traced through the $^{15}N/^{14}N$ ratio (Caselli & Ceccarelli 2012), the temperature dependence of the location of the different nitrogen carriers, compared to the water and methanol snow lines, is a fundamental step to understand planets formation (Vernazza et al. 2017). To support observations and in situ space missions, like the Rosetta mission, it is important to characterize the desorption process of species, in addition to their temperature dependent IR spectra. So far, to our knowledge, only the desorption of the ammonium cyanide salt, $NH_4^+CN^-$, have been quantitatively studied (Noble et al. 2013).

In this paper, we conducted a laboratory study of the desorption of ammonium formate, $NH_4^+HCOO^-$, and ammonium acetate, $NH_4^+CH_3COO^-$, salts with and without a water ice substrate. We performed temperature-programmed desorption experiments to study both the desorption mechanism and the reactivity of the two salts during the desorption process, using an experimental setup mimicking the interstellar conditions. We describe the ultra-high vacuum apparatus along with the experimental protocol and data analysis in Section 2. In Section 3 we present the results of our two complementary techniques, infrared and mass spectroscopy. We discuss the results and try to answer the following questions: what are the binding energies? When are ammonium salts formed and destroyed? Is it the ions or neutrals that mostly desorb? Is the presence of water affecting the formation and desorption of salts? In Section 4, we discuss the astrophysical implications of ammonium salts desorption, especially in the context of planetary formation.
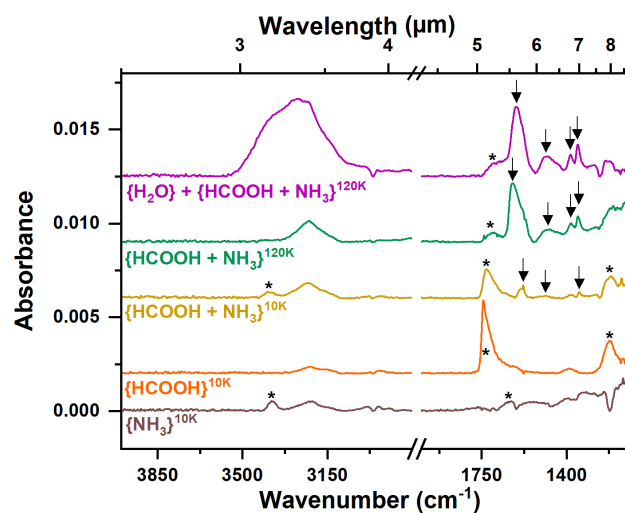
2. Experimental

All experiments were conducted with the novel multi-beam ultra-high vacuum (UHV) apparatus called VENUS (VErs les NoUvelles Synthèses) based in the LERMA laboratory at the CY Cergy Paris University. VENUS has been described in details elsewhere Congiu et al. (2020) and only a brief account of the most relevant aspects of the experimental setup is given here. The experiments were carried out under UHV conditions (base pressure 2×10^{-10} hPa at 10 K) in a stainless steel chamber. The sample holder is made of a circular copper mirror coated with gold, and mounted onto the cold head of a closed-cycle He cryostat. The sample temperature can be controlled in the 7 – 400 K range by using a regulated resistive heater clamped on the back of the sample holder. The ice analogs were prepared from gas condensation of molecular effusive beams aimed at close normal incidence onto the gold substrate or, in specific cases, on a slab of water ice deposited on the sample holder. The evolution of the ice during deposition was monitored by Fourier transform reflection absorption infrared spectroscopy (FT-RAIRS) using a Vertex 70 spectrometer. Once the desired ice thickness of a few layers was reached, the sample was analyzed by means of the Temperature-Programmed Desorption (TPD) technique.

The TPD technique is used to identify the nature of desorbing species by mass and it is also a powerful method to derive binding energies of molecules adsorbed on surfaces. The method consists in increasing gradually the temperature of the surface at a constant heating rate while registering the desorption signal (a mass spectrum) as a function of sample temperature. VENUS is equipped with a Hiden 51/3F quadrupole mass spectrometer (QMS) placed 5 mm in front of the sample to monitor gas phase species in the UHV chamber.

Table 1. List of experiments and corresponding ice composition, thickness and deposition temperature.

Exp.	Ice composition	Thickness (monolayers)	T_{dep} (K)
i	NH_3	6.5	10
ii	$HCOOH$	4.5	10
iii	$HCOOH : NH_3$	3.7 : 4.5	10
iv	$HCOOH : NH_3$	3.7 : 4.5	120
v	$H_2O : HCOOH : NH_3$	15 : 3.7 : 4.5	120
vi	CH_3COOH	2.5	120
vii	$H_2O : CH_3COOH$	15 : 2.5	10
viii	$CH_3COOH : NH_3$	2.5 : 4.5	120

The desorption characteristics of pure ices and ice mixtures (NH_3:$HCOOH$ and NH_3:CH_3COOH) were investigated. An overview of the performed experiments is reported in Table 1. For the mixtures (Exp. iii, iv, v, vii, viii), the proportion of ammonia was set to be 20% higher which should favor the reaction with the acid, the same will occur in the ISM conditions since ammonia is an abundant constituent of interstellar ices which correspond to a fraction of a few percent of the ice, whereas acids are suspected to be around one percent (Boogert et al. 2015). The heating ramp was set to 0.2 K s^{-1} for all experiments, with each TPD starting from the deposition temperature. In the figures of this paper, the notation $\{sampleA + sampleB\}^T_{A:B}$ is used to indicate that the gases were co-deposited at temperature T and the estimated final thickness of each sample is A : B, expressed in monolayers (ML), where 1 ML = 10^{15} molecules cm^{-2}. As an example $\{HCOOH + NH_3\}^{10K}_{3.7:4.5ML}$ means that we have co-deposited 3.7 ML of HCOOH and 4.5 ML of NH_3 at 10 K on the

Fig. 1. RAIRS spectra of experiments related to the formation of ammonium formate. The bands highlighted by stars (*) correspond to the absorption features of neutral molecules, NH_3 and HCOOH. When these two species are co-deposited, vibrations of the molecular ions (NH_4^+ and $HCOO^-$) appear (↓), suggesting the formation of ammonium formate.

gold-coated target. The average H_2O ice coverage in ISM is supposed to be from a sub-monolayer regime up to 30 ML (Potapov et al. 2020), or even to a few hundreds according to some authors. Here the final thickness of the samples does not exceed 10 ML in the experiments without water and 25 ML in the experiment with water (Exp. v), which is a good approximation to the ISM conditions.

3. Results

3.1. Desorption of ammonium formate

3.1.1. Pure ices: HCOOH and NH_3

The IR spectra of pure NH_3 and HCOOH are showed in Fig. 1. The attributed absorption bands are listed in Table 2. Both spectra were recorded at the end of the deposition of each species carried out at 10 K. The film thickness in all experiments corresponds to a few monolayers (6.5 ML for NH_3 and 4.5 ML for HCOOH), for this reason the IR spectrum recorded is at the limit of signal-to-noise ratio of the spectrometer. The IR spectrum of solid NH_3 is well documented in the literature (D'Hendecourt & Allamandola 1986; Sandford & Allamandola 1993; Noble et al. 2013; Bouilloud et al. 2015), and here we can distinguish two important bands: the NH_3 ν_3 and ν_4 modes at 3375 cm^{-1} and 1641 cm^{-1}, respectively, indicated by stars (*) on the figure. There is also a feature around 3200 cm^{-1} attributed to crystalline water that grows on the window of the IR detector itself, located outside of the experimental chamber. This band is likely to affect the spectrum in its surroundings so extreme care was taken in analyzing features in the vicinity of 3200 cm^{-1} under our experimental conditions.

The IR properties of HCOOH were studied in details in Bisschop et al. (2007). The formic acid spectrum in Fig. 1 displays two bands at 1743 and 1222 cm^{-1}. The prominent peak at 1743 cm^{-1} originates from the ν(C=O) stretching vibration, while the band at 1222 cm^{-1} is due to the ν(C–O) stretching mode of HCOOH.

Table 2. IR band assignments (cm^{-1}) of NH$_3$, HCOOH, and CH$_3$COOH as pure ices and as ice mixtures (D'Hendecourt & Allamandola 1986; Sandford & Allamandola 1993; Noble et al. 2013; Bouilloud et al. 2015; Bisschop et al. 2007; Hellebust et al. 2007; Gálvez et al. 2010; Bahr et al. 2006; Ito & Bernstein 1956; Sivaraman et al. 2013).

Mode	NH$_3$	HCOOH	HCOOH:NH$_3$		H$_2$O:HCOOH:NH$_3$	CH$_3$COOH		CH$_3$COOH:NH$_3$
	(i)	(ii)	(iii)	(iv)	(v)	(vi)	(vii)	(viii)
NH$_3$ (ν_4, NH bend)	1641	-	-	-	-	-	-	-
NH$_3$ (ν_3, NH bend)	3375	-	3380	-	-	-	-	-
HCOOH (ν, C–O st)	-	1222	1216	-	-	-	-	-
HCOOH (ν, C=O st)	-	1743	1730	1710	1697	-	-	-
HCOO$^-$ (ν_4,C–O s-st)	-	-	1346	1353	1353	-	-	-
HCOO$^-$ (δ, CH st)	-	-	1382	-	1384	-	-	-
NH$_4^+$ (ν_4, NH bend)	-	-	1487	1475	1482	-	-	1500
HCOO$^-$ (ν_2, C–O a-st)	-	-	1579	1621	1608	-	-	-
CH$_3$COOH (ν, C=O st)	-	-	-	-	-	1724	1716	1700
CH$_3$COOH (ν, C=O a-st)	-	-	-	-	-	1643	1655	-
CH$_3$COOH (δ, CH$_3$ a-st)	-	-	-	-	-	1413	1428	-
CH$_3$COOH (ν, C–O st)	-	-	-	-	-	1307	1290	1292
CH$_3$COO$^-$ (ν, C=O st)	-	-	-	-	-	-	-	1575
CH$_3$COO$^-$ (ν, C=O a-st)	-	-	-	-	-	-	-	1428

Figure 2 presents the TPD profiles of the experiments involving HCOOH and NH$_3$. The left panels, (a) and (c), show the desorption of pure species deposited directly onto the gold substrate. In the case of pure NH$_3$, in addition to the parent ion NH$_3^+$, the fragment ion NH$_2^+$ was also monitored by the quadrupole mass spectrometer. The resulting TPD mass spectrum shows the desorption of the parent molecule (m/z = 17) and the fragment at m/z = 16, with both maxima of desorption peaking at around 94 K. These two mass signals always present a constant ratio of ~2:1. We point out that the ratio of fragments depends on the kinetic energy of ionizing electrons, which is set to 30 eV in our spectrometer, thus lower than the typical value of 70 eV. The value of 30 eV was chosen to optimize the stability of the system and reduce fragmentation.

In the interstellar medium, a key parameter that governs the chemical abundance in the solid and in the gas phase is the residence time of species on the dust-grain surface determined by their desorption rate. In an out-of-equilibrium treatment desorption from a surface, considering an open volume, the rate of the desorption, $\frac{dN}{dT}$, can be described by the Wigner-Polanyi equation:

$$-\frac{dN}{dt} = k_{des}N^n \tag{1}$$

where k_{des} is the desorption rate constant, N is the number of adsorbed molecules, n is the order of the reaction and the minus sign accounts for the loss of molecules from the surface. For a thermal desorption, k_{des} depends on the binding energy of the specific species adsorbed, and is given by an Arrhenius law:

$$-\frac{dN}{dt} = A \exp\left(-\frac{E_{bind}}{RT}\right)N^n. \tag{2}$$

Here A is a pre-exponential factor, E$_{bind}$ is the binding energy of the species, R is the gas constant and T is the surface temperature. During a TPD experiment the sample is heated at a constant rate $\frac{dT}{dt} = \beta$ and Equation (2) can be rearranged in terms of the temperature and β to derive the kinetic parameters, A and E$_{bind}$, from the experimental data:

$$-\frac{d\theta}{dT} = \frac{A}{\beta} \exp\left(\frac{-E_{bind}}{RT}\right)\theta^n, \tag{3}$$

where $\frac{d\theta}{dT}$ is the desorption rate (ML K^{-1}), A a pre-exponential factor in s^{-1}, for a first order desorption $n = 1$, θ is the surface coverage in ML, E$_{bind}$ is the binding energy for desorption (J mol^{-1}), R is the gas constant (J K^{-1} mol^{-1}), and T is the temperature of the surface (K).

To obtain the binding energies and pre-exponential factors from the TPD curves from Equation 3, a standard minimization of χ^2 is used, which reflects the sum of the squares of the differences between the experimental profiles and calculated ones (Acharyya et al. 2007). The values of desorption rate as a function of the temperature and the surface coverage were obtained directly from the experimental data. In order to work with only the binding energy as a free parameter during the fit, we used the method proposed by Noble et al. (2013), where the pre-exponential factor value is fixed. We start assuming that the lattice vibrational frequency of the solids is 10^{13} s^{-1}. However, if the number of vibrational modes of the molecule increases, as is the case of molecules with a larger number of atoms, the lattice vibrational frequency also tends to increase and the value of the pre-exponential factor has to be optimized and increased gradually in order to reduce the χ^2 value.

Using this approach, the couple binding energy and pre-exponential factor were estimated assuming a 1st-order process (n = 1) for pure NH$_3$: E$_{bind}$ = 25.5 ± 0.1 kJ mol^{-1} and A = 1.0 ± 0.2 × 10^{13} s^{-1}. These values are consistent with those previously published in the literature (Ulbricht et al. 2006; Noble et al. 2013; Martín-Doménech et al. 2014) and are reported with our other values in Table 3.

Panel c) of Figure 2 displays the TPD curve of pure formic acid. Two desorption components, at 138 and 152 K, can be distinguished in the spectra possibly because of the formation of different phases of formic acid with an amorphous and a crystalline structure. The desorption behavior of formic acid was studied previously by Bahr et al. (2005); Hellebust et al. (2007) and recently by Chaabouni et al. (2020). Dimeric HCOOH can be present in the gas phase and remains in this form as an amorphous film during deposition being later converted into a crystalline film during annealing (Hellebust et al. 2007).

Formic acid dissociates into several fragments in our experiments, but here only the three major fragments are shown (Fig. 2.c). The fragment at m/z = 46 is related to the ionized parent molecule HCOOH$^+$, while the fragment of higher inten-
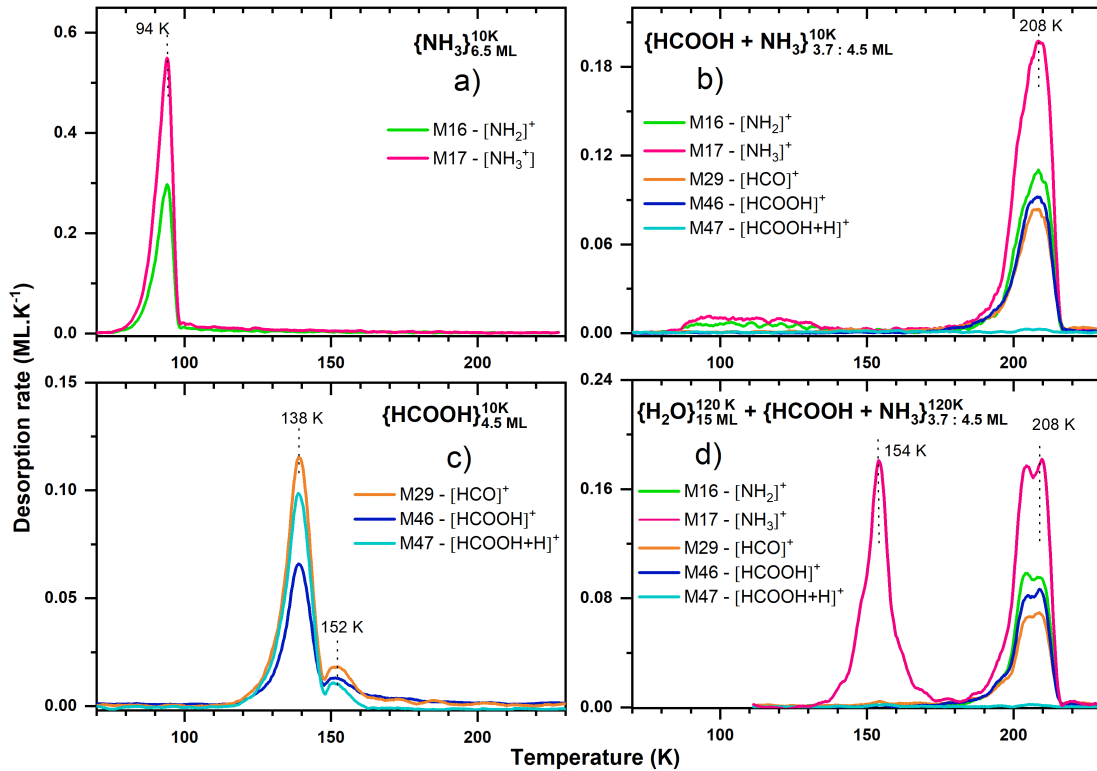
Fig. 2. Left panels: TPD spectra of (a) pure NH_3 and (c) pure HCOOH. Right panels: TPD spectra of mixed NH_3 and HCOOH (b) without and (d) with a substrate of water. The desorption component around 208 K traces the desorption of $NH_4^+HCOO^-$ and the ratio between its fragments, similar to those of pure molecules, indicates the dissociation of the salt during the desorption process back into the components, NH_3 and HCOOH.

Table 3. Kinetic parameters for the desorption of ammonium salts and their neutral components compared with available reference values. Errors arise from the spread of the fit values.

Molecule	E_{bind} (kJ/mol)	A (s^{-1})	Reference
NH_3	25.5 ± 0.1	$1.0 \pm 0.2 \times 10^{13}$	This work
	26 ± 1	$1.0 \pm 0 \times 10^{13}$	Noble et al. (2013)
HCOOH	38.3 ± 0.1	$1.1 \pm 0.2 \times 10^{13}$	This work
	$27.8 - 47.7$	1.0×10^{13}	Chaabouni et al. (2020)[a]
	$27.1 - 49.1$	1.0×10^{13}	Shiozawa et al. (2015)[a]
CH_3COOH	46.8 ± 0.2	$1.1 \pm 0.2 \times 10^{13}$	This work
	55 ± 2	$8 \times 10^{17\pm3}$	Burke et al. (2015)
$NH_4^+HCOO^-$	68.9 ± 0.1	$7.7 \pm 0.6 \times 10^{15}$	This work
$NH_4^+CH_3COO^-$	83.0 ± 0.2	$3.0 \pm 0.4 \times 10^{20}$	This work

[a] Values after the conversion with A fixed at 10^{13} s^{-1}.

sity in the TPD spectra (at m/z = 29) is due to the loss of a hydroxyl group, -OH, a common pattern in carboxylic acids that gives HCO^+ fragments in the case of HCOOH. The fragment at m/z = 47 can be attributed to the formation of dimeric formic acid that break up resulting in $HCOOH-H^+$ species (Chaabouni et al. 2020).

The binding energy and the pre-exponential factor derived using Equation 3 for formic acid are $E_{bind} = 38.3 \pm 0.1$ kJ mol^{-1} and $A = 1.1 \pm 0.2 \times 10^{13}$ s^{-1}. To compare the binding energy value with the previously published results of the kinetic parameters of formic acid, we used the method described in Chaabouni et al. (2018). Since there is a relation between A and E_{bind}, we can use the same pre-exponential factor ($A = 10^{13}$ s^{-1}) and convert the values provided by Shiozawa et al. (2015) and Chaabouni et al. (2020) to compare with our results. From

Table 3, we can see that the binding energy values for formic acid found in these different studies are similar, and that under our conditions of thickness and on a gold substrate, the values we find are in between the values corresponding to the HCOOH monomer and dimer. This may indicate that in our experiment, HCOOH is desorbing from the surface as a mixture of both forms of HCOOH.

3.1.2. Mixed ices: HCOOH + NH_3

To form $NH_4^+HCOO^-$ salt, HCOOH and NH_3 gases were injected into the VENUS main chamber using two separated molecular beams, and co-deposited on the gold surface held at two different temperatures, 10 and 120 K. The flux of the NH_3

beam was set to be 20% in excess compared to the HCOOH beam, which should favor the reaction between the two species.

Figure 1 show the IR spectra of HCOOH + NH$_3$ deposited at 10 and 120 K (displayed in yellow and green, respectively). In the experiment conducted at 10 K, it is possible to see absorption features of both species in their neutral form, highlighted in the figure with stars (*). Comparing this spectrum with the spectra of pure NH$_3$ and HCOOH, we can distinguish the presence of NH$_3$ due to the 3380 cm^{-1} absorption band, while in the low wavenumber range two features can be attributed to HCOOH: the high intensity absorption band at 1730 cm^{-1} due to the C=O stretch and the broad band at 1216 cm^{-1} due to C−O stretch. Other three bands can be distinguished in the spectrum, indicated by arrows, and are consistent with the salt bands associated with the formation of ammonium formate (NH$_4^+$HCOO$^-$). A broad band of low intensity around 1487 cm^{-1} is attributed to the ν_4 NH bending mode of NH$_4^+$ ions, and two other absorption bands are found related to HCOO$^-$, the ν_4 C−O asymmetric and symmetric stretch at 1579 and 1346 cm^{-1} (Hellebust et al. 2007; Gálvez et al. 2010; Bergner et al. 2016). The presence of ionic features at 10 K indicates that the samples have undergone a reaction during the deposition phase. The proton-transfer between HCOOH and NH$_3$ is an acid-base reaction that produces NH$_4^+$HCOO$^-$ and is characterized by a low-activation energy that allows the reaction to occur at cryogenic temperatures (Theulé et al. 2013):

$$HCOOH + NH_3 \longrightarrow NH_4^+HCOO^- \qquad (4)$$

In the experiment where the mixture HCOOH + NH$_3$ was co-deposited at 120 K the IR features related to the ion species are predominant (Fig. 1, green profile). The most intense band is due to the HCOO$^-$ ν_4 C−O symmetrical stretch which was blue-shifted to 1621 cm^{-1} compared to the spectrum deposited at 10 K. Additionally, the other salt bands present at 10 K become stronger and, in general, red-shifted: the broad band at around 1475 cm^{-1} of the NH$_4^+$ ν_4 NH bending mode and the ν_4 C−O symmetric stretch at 1353 cm^{-1}. We point out that in the 120 K-deposition experiment NH$_3$ molecules cannot stick and accumulate on the surface, since their desorption flux is orders of magnitude higher than their accretion flux. Therefore, only ionic forms can be kept on the surface. Despite the short residence time of NH$_3$ (1/k$_{des}$ = 0.08 s) at 120 K we observe an efficiency of formation of salts equal to one, normalized to the HCOOH partner. This implies that the formation rate is much higher than the desorption rate. Actually, the gradual temperature increase during a TPD favors the reaction between the components producing ammonium formate (Hellebust et al. 2007; Gálvez et al. 2010; Bergner et al. 2016).

The right panels of Figure 2 display the TPD spectra of experiments involving HCOOH and NH$_3$ mixtures deposited at 10 K without water (b) and at 120 K with water (d). The fragments displayed in the TPD curves of mixed ices are the same showed for pure species. In the experiment performed at 10 K (Fig. 2(b)) the desorption occurs in two steps. A first desorption starts at 80 K and only fragments m/z = 16 and 17 have a relevant intensity. This peak can be attributed to the desorption of NH$_3$ in excess, that did not react with HCOOH to produce ammonium formate during the warm-up. The second feature shows the desorption of fragments at m/z = 16, 17, 29 and 46, and occurs at around 208 K. This component desorbing at temperatures higher than the desorption of pure HCOOH and pure NH$_3$ is attributed to the desorption of ammonium formate. The desorption energy estimated using Eq. 3 for ammonium formate is E$_{bind}$ = 68.9 ± 0.1 kJ mol^{-1} with a pre-exponential factor A = 7.7 ± 0.6

$\times 10^{15}$. Since the stoichiometry of reaction 4 is 1 : 1, the reaction yield can be estimated considering the limiting reactant HCOOH consumed during the experiment. No residual formic acid desorbs at high temperature, which suggests that all formic acid available reacted with ammonia to produce ammonium formate. Moreover, the areas of TPD peaks confirm mass conservation of the deposited species, indicating that there was no loss prior to desorption and that no change in detection efficiency of the QMS occurred.
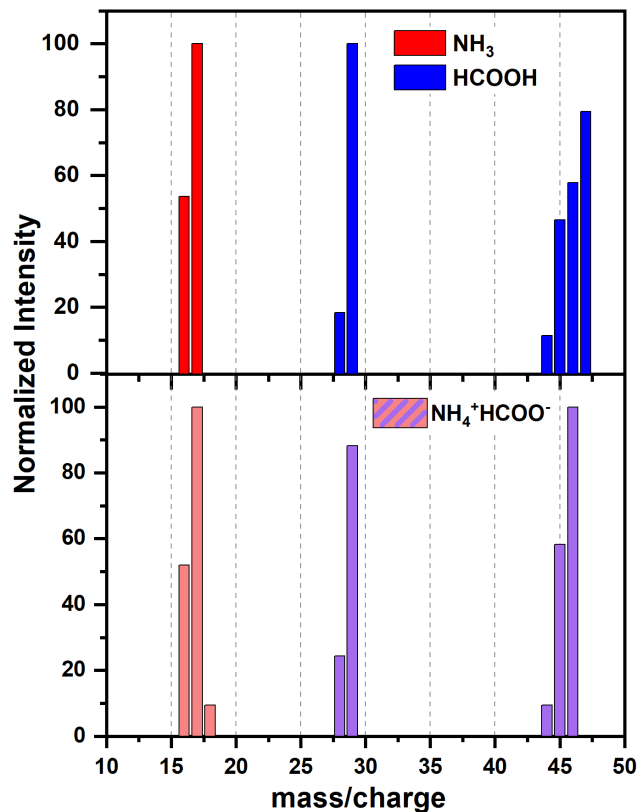

Fig. 3. Mass spectra of NH$_3$, HCOOH and NH$_4^+$HCOO$^-$. Intensities are normalized to the most intense of the peaks for NH$_3$ (m/z = 17) and HCOOH (m/z = 29). For NH$_4^+$HCOO$^-$, the fragments corresponding to ammonia are normalized to the most intense of the peaks (m/z = 17) and the ones from formic acid to the second peak most intense (m/z = 46).

The desorption profile of ammonium formate also indicates that the salt dissociates releasing neutral ammonia and formic acid to the gas phase at temperatures higher than the desorption temperatures of the pure species. This argument is corroborated because the same fragmentation pattern shows up both in the mass spectra of pure HCOOH and pure NH$_3$ and in the TPD spectrum of ammonium formate (Fig. 3). In particular, we observe the exact ratio between mass 17 and mass 16, in addition to the conservation of the total amount deposited. This would have been impossible if a substantial fraction of ammonia had desorbed in the form of NH$_4^+$, or directly in the form of salt, which implies a different cracking pattern.

The mechanisms of sublimation of ammonium salts were investigated through NH$_4^+$Cl$^-$ systems by Zhu et al. (2007). The study found that the rate-controlling step in the dissociation of NH$_4^+$Cl$^-$ salt is the formation and desorption of the [NH$_3 \cdots$ HCl] complex that later dissociates without a distinct barrier into NH$_{3(g)}$ and HCl$_{(g)}$. Although in our experiment we cannot measure the formation of a [NH$_3 \cdots$ HCOOH] complex,

we observe that the salt dissociates and releases the neutral components into the gas phase:

$$NH_4^+HCOO^-_{(s)} \rightleftharpoons NH_{3(g)} + HCOOH_{(g)} \qquad (5)$$
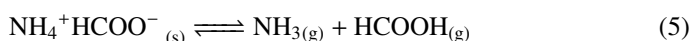
Additionally, only the fragment at m/z = 47 that is associated with the cracking pattern of HCOOH dimers is absent in the TPD spectrum of ammonium formate, suggesting that formic acid does not re-associate into its dimeric form in the gas-phase before reaching the QMS.

3.1.3. Influence of water ice mantles on the desorption of ammonium salts

The experiment involving the HCOOH + NH₃ mixture in the presence of water carried out at 120 K allows us to evaluate the effects of water ice mantles on the desorption of ammonium salts. The RAIRS spectrum of this experiment does not show a significant difference of the absorption features in the spectral interval between 2000 cm⁻¹ and 1100 cm⁻¹. The main difference is seen at around 3000 cm⁻¹ and shows the characteristic broad band of water due to the −OH stretch.

Panel d) of Figure 2 shows the desorption rate of ammonium formate on a water ice substrate deposited at 120 K. At around 154 K water desorption reaches its maximum as we can see looking at the ion at m/z = 17, which is 14% of that at m/z = 18 (not shown for clarity). The second desorption peak at around 208 K exhibits the same characteristics as the mass spectra recorded in experiments performed on the bare gold target from 10 or 120 K. The water substrate does not influence the TPD profiles of NH₄⁺HCOO⁻, and the salt desorbs as a semi-volatile species after complete desorption of the water ice substrate.
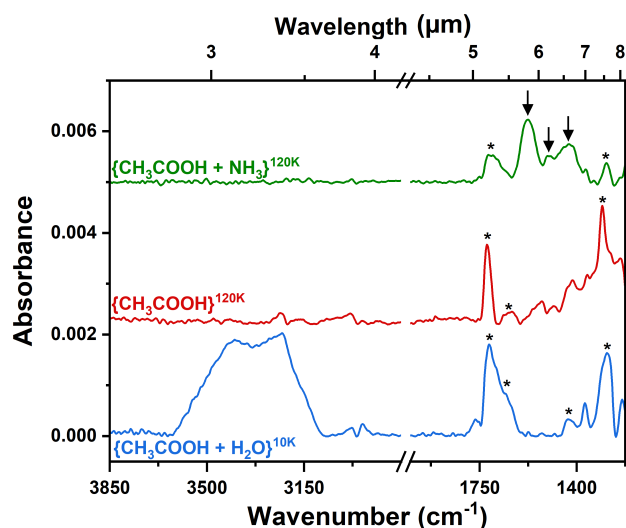
3.2. Formation and desorption of ammonium acetate

3.2.1. Pure CH₃COOH

The IR spectra of pure acetic acid deposited at 10 and 120 K are displayed in Figure 4. The influence of the deposition temperature and the effect of two substrates (gold and water ice) were evaluated. In the presence of water, acetic acid deposited at 10 K displays three IR bands at low frequencies assigned to the vibration of the carbonyl group. Two bands related to the ν(C=O) absorption feature at 1716 cm⁻¹ and 1655 cm⁻¹ are observed convoluted. These bands and the absorption at 1290 cm⁻¹ are attributed to acetic acid dimers following the values reported in previous studies (Bahr et al. 2005; Hellebust et al. 2007). When the deposition temperature increases from 10 to 120 K the bands become narrower and resolved. The 1643 cm⁻¹ feature has a broad absorption and low intensity, while the 1722 cm⁻¹ and 1290 cm⁻¹ bands are sharper and predominate the spectra being the most intense bands.

The upper panel in Figure 5 shows the desorption profile of CH₃COOH and NH₃ for comparison, already discussed in the previous section. Acetic acid breaks up into several species, the most intense fragment corresponding to m/z = 43, and is attributed to CH₃CO⁺ generated after the loss of its hydroxyl group. The fragments related to the parent molecule, CH₃COOH⁺ and the dimer, CH₃COOH−H⁺, are the traces for m/z = 60 and 61.

The calculated values of binding energy and pre-exponential factor for the desorption of acetic acid are E_{bind} = 46.8 ± 0.2 kJ mol⁻¹ and a pre-exponential factor A = 1.1 ± 0.2 × 10¹³ s⁻¹,

Fig. 4. RAIRS spectra of experiments involving the formation of ammonium acetate. The highlighted bands using stars are related to absorption features of neutral acetic acid. When NH₃ and CH₃COOH are co-deposited, the bands related to NH₄⁺CH₃COO⁻ appear (indicated by arrows.)

that are in a good agreement with the values reported previously in the literature (Burke et al. 2015).

3.2.2. Mixed ices: CH₃COOH + NH₃

The IR spectrum of the CH₃COOH + NH₃ mixture deposited at 120 K is showed in Figure 4. So far, to our knowledge, the IR spectrum of ammonium acetate has never been reported in the literature, so we used the IR bands of sodium acetate and methyl acetate to identify the salt features (Ito & Bernstein 1956; Sivaraman et al. 2013). The ν(C=O) asymmetrical and symmetrical stretch at 1575 and 1428 cm⁻¹ are attributed to CH₃COO⁻ ions. The IR spectrum of sodium and methyl acetate do not display any prominent absorbance in the range between 1490 - 1600 cm⁻¹, hence we attribute the 1500 cm⁻¹ absorbance to the ν(N−H) bending mode of NH₄⁺, corresponding to the same pattern seen in the spectrum of ammonium formate.
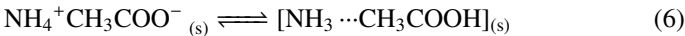
The bottom panel of Figure 5 presents the TPD profile of the CH₃COOH + NH₃ mixture deposited at 120 K. The spectra do not display traces of ammonia or acetic acid desorbing as pure species at temperatures below 180 K. The desorption peak at around 200 K is attributed to the desorption of ammonium acetate. As discussed for the TPD spectra of ammonium formate, the fragments highlighted are the same showed for pure acetic acid and ammonia and indicate that the salt dissociates releasing the base and the acid in their neutral form into the gas phase before being detected by the QMS. In the case of ammonium acetate, the fragment at m/z = 61, corresponding to one of the fragments of CH₃COOH dimers, presents a significant desorption rate, which indicates that dimeric acetic acid could form after the dissociation of the salt.

The binding energy for ammonium acetate is estimated to be E_{des} = 83.0 ± 0.2 kJ mol⁻¹ with a pre-exponential factor A = 3.0 ± 0.4 × 10²⁰ s⁻¹. The high value of the pre-exponential factor is a classical trend observed when molecular complexity increases (Tait et al. 2005). Quite astonishingly, it is observed that the desorption of ammonium acetate occurs before that of ammonium formate. Usually, the larger the molecular complexes are, the greater the energy of their interaction with the surface, sim-
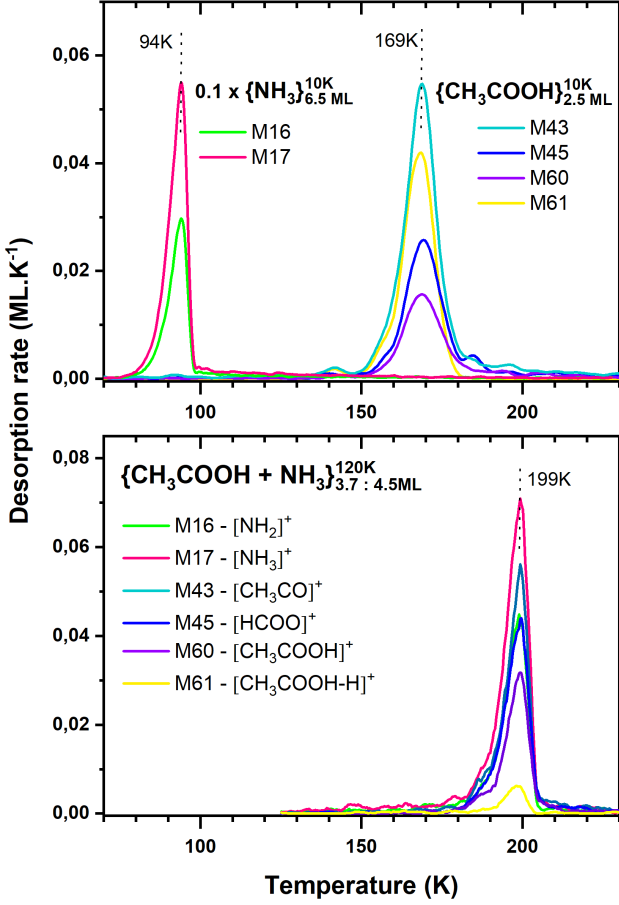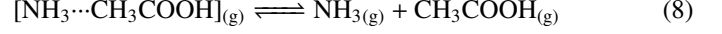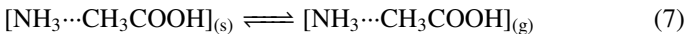
Fig. 5. Top panel: TPD spectra of NH_3 and CH_3COOH. Bottom panel: TPD spectrum of $NH_4^+CH_3COO^-$, the sharp profile of the desorption is linked with a high pre-exponential factor and may indicate that the dissociation of the salt is at the origin of the desorption process.

$$[NH_3\cdots CH_3COOH]_{(g)} \rightleftharpoons NH_{3(g)} + CH_3COOH_{(g)} \qquad (8)$$

The pre-exponential factor hides several physical mechanisms such as a multi-step desorption composed of several elementary activated processes, or a multi-site diffusion energy, resulting in a high (and sometimes temperature-dependent) value of the factor A. Figure 6 shows the tentative fit of the acetate TPD trace using a pre-exponential factor $A = 10^{13}$ s^{-1}, used for the other molecules, and the best fit obtained using $A = 10^{20}$ s^{-1}. The fact we are measuring a (probably multi-step) chemical reaction, rather than a molecular desorption, can explain the high value of the calculated pre-exponential factor.

Fig. 6. The TPD curve of ammonium acetate is better fitted using a high value of the pre-exponential factor, $A = 10^{20}$ s^{-1}, instead of $A = 10^{13}$ s^{-1} used for the other molecules. The origin of this difference is probably because we are not measuring only the desorption process, but a multi-step reaction that includes the dissociation of ammonium acetate.
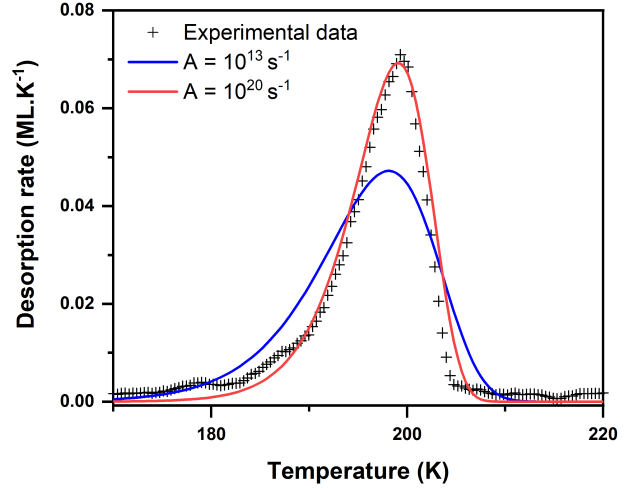
ply because the multiplicity of their interaction increases. This is observed, for example, in the TPD of pure formic and acetic acids, although it is a general rule of thumb (e.g., methanol has a lower binding energy than ethanol, which is lower than that of propanol). This is not what is observed for the salts, and it probably indicates that the desorption of salts occurs concurrently with dissociation into their neutral components. The binding energy would be a kind of measure of the intrinsic stability of the salt, so the ammonium formate is more stable than ammonium acetate, which is probably also related to the stronger acidity character of formic acid with respect to acetic acid, and therefore to its greater propensity to donate a proton. The ability to transfer the proton in the forward or backward reaction is translated in the logarithm of the acidity constant (pK_a) of the species. This proves that what we are actually measuring is the activation energy of the endothermic backward reaction rather than the desorption energy:

$$NH_4^+CH_3COO^-_{(s)} \rightleftharpoons [NH_3\cdots CH_3COOH]_{(s)} \qquad (6)$$

Once the backward reaction has occurred, the neutrals, which should have desorbed long before (at 199 K t_{res} = 4.9 10^{-7} s for NH_3 and t_{res} = 1.13 ms for HCOOH), desorb very rapidly at this temperature:

$$[NH_3\cdots CH_3COOH]_{(s)} \rightleftharpoons [NH_3\cdots CH_3COOH]_{(g)} \qquad (7)$$

4. Discussion

Observations of the N-bearing carriers (the NH_3/NH_4^+ hydride, the nitrogen ^{14}N/^{15}N or the hydrogen H/D isotopic ratios in N-bearing hydrides) give information on the chemical evolution of the solar system: from the proto-solar nebula, to the solar system bodies and/or planetary atmospheres (Caselli & Ceccarelli 2012). Thus, it is important to retrace the chemical journey of the main N-carriers from the pre-solar nebula to the solar system bodies. NH_3 and NH_4^+ are the main observed carriers in ice, although they account for less than 10 % of the overall nitrogen elemental budget (Öberg et al. 2011). These two species behave differently with respect to the desorption.

According to Viti et al. (2004)'s classification, NH_3 is a H_2O-like molecule, whose desorption is mostly co-desorption with water ice, and as such it can be modeled following the same pattern as the desorption of the water ice mantle. NH_4^+ is a semi-volatile/refractory species (the term refractory applying to species incorporated in the dust grain by a covalent bond and sublimating at much higher temperatures than that of water ice), and the characteristics of its desorption have been measured in this paper. NH_3 can be easily converted into NH_4^+ by a set of thermal reactions involving proton transfer (Theulé et al. 2013) in the temperature range found in the warm layers of the disk or

even in the disk mid-plane for a low-mass protostar, or in any region of the disk in the case of a high-mass protostar.

We will consider three scenarios: *i.* the desorption of NH_3 ($A = 1.0 \times 10^{13}$ s^{-1}, E = 25.5 kJ mol^{-1}) desorbing from a surface as a pure species; *ii.* complete co-desorption of NH_3/NH_4^+ with amorphous water ice ($A = 10^{18}$ s^{-1}, E = 54.5 kJ mol^{-1}) that coincides with desorption from the water snow-line location in the disk; *iii.* delayed desorption of NH_4^+ ($A = 7.7\ 10^{15}$ s^{-1}, E = 68.9 kJ.mol^{-1}, calculated in this work) corresponding to desorption from an "ammonium-line". We can see in Fig. 7 that, depending on the parameters used in the ammonia/ammonium desorption, the amount of nitrogen stored in solar system bodies located beyond the snow-line can be considerably different, as well as the implications concerning the formation of the solar system. Since ammonia is the only base, lots of species present in the ice can undergo either an acid-base reaction or a nucleophilic reaction with it (Theulé et al. 2013). As a result, most of the NH_3 present in the ice should be locked in a more complex species such as an ammonium salt, which implies a delayed desorption with respect to pure NH_3.
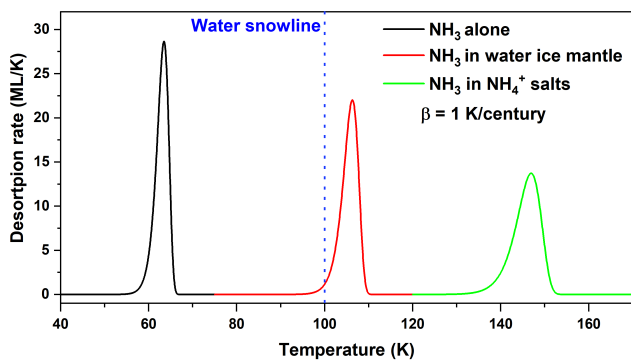
Fig. 7. TPD simulation showing that ammonia can desorb in more than one temperature range depending on its chemical nature and chemical environment. If ammonia is locked in ammonium salts, it desorbs at higher temperature with respect to the water snow-line. The heating rate of this simulation is $\beta = 1$ K/century, a typical estimation for high-mass stars (Viti & Williams 1999; Viti et al. 2004). For low-mass stars, the heating rate would be slower and the effect of delay even more pronounced.

Another important aspect lies in the mild temperature chemistry of semi-volatile species. While the chemistry of the parent molecules (NH_3, HNCO, HCOOH, CO_2) have been extensively studied either under conditions present in molecular clouds or during the warming resulting from a star formation process (Raunier et al. 2004; Bossa et al. 2008; Bertin et al. 2009; Bergner et al. 2016), the chemistry of their products, the salts, have not been studied to a significant extent under conditions preponderant beyond the snow-line. Indeed, all molecules present in the icy mantles were supposed to co-desorb with water at the snow-line or at lower temperatures if considered volatile species. The presence of semi-volatile species beyond the snow-line, at distances smaller than about 3 AU from the protostar, enables: *i.* a mild (around 200 K) thermal chemistry; *ii.* a dry (water-free) photo-chemistry; *iii.* a dry ion/electron-induced chemistry due to the solar winds. Since these three energetic processes are stronger beyond the snow-line, semi-volatile molecules are more likely to be included in the soluble or insoluble matter of meteorites. As an example, ammonium perchlorate salt, $NH_4^+ClO_4^-$, produces hydroxylamine, NH_2OH, upon electron radiolysis (Góbi et al. 2017).

An interesting finding of this work is that most of the NH_4^+ is converted into NH_3 by a back transfer of the proton during the desorption processes, and consequently the thermal reaction $NH_4^+HCOO^- \rightarrow NH_2CHO + H_2O$ (Lorin & al. 1864) activation barrier is too high to produce formamide in detectable amounts. This is how historically formamide was produced industrially from the heating of ammonium formate (Lorin & al. 1864). In a forthcoming paper, we will address the reactivity of salts upon H-atom bombardment.

5. Conclusion

In this work, we presented an experimental study of the desorption of two ammonium salts, ammonium formate, $NH_4^+HCOO^-$, and ammonium acetate, $NH_4^+CH_3COO^-$, in an astrophysically relevant environment. Based on our results, we conclude that:

(i) Using IR spectra of mixtures containing NH_3 and an organic acid, HCOOH or CH_3COOH, we showed that ammonium salts are efficiently produced at temperatures as low as 10 K. They undergo a complete reaction with the increase in temperature, with or without the presence of water, which does not affect the desorption process under our experimental conditions.

(ii) For both salts the ammonium NH_4^+ transfers back its proton to the corresponding anion to release ammonia and the corresponding acid (HCOOH and CH_3COOH). No complex organic molecules (e.g., formamide, acetamide, urea) are formed during the desorption process. Ammonia is the only N-bearing species that sublimates so nitrogen atoms return to the gas phase locked in ammonia at temperatures higher than that of desorption of water ice.

(iii) Desorption of ammonium salts follows a first-order Wigner-Polanyi law. The kinetic parameters of the desorption of ammonium salts were examined. Both $NH_4^+HCOO^-$ and $NH_4^+CH_3COO^-$ desorb following a first-order desorption with rate constant $k_{des} = 7.7 \pm 0.6 \times 10^{15} \times \exp(-68.9 \pm 0.1/RT)$ for $NH_4^+HCOO^-$, and $k_{des} = 3.0 \pm 0.4 \times 10^{20} \times \exp(-83.0 \pm 0.2/RT)$ for $NH_4^+CH_3COO^-$. Both salts are semi-volatile species as they desorb at temperatures higher than that of the desorption of water ice, although lower than room temperature.

(iv) In a mixture of water ice and ammonium salt, in which the salt constitutes a few percent of the total, the fraction of $NH_4^+HCOO^-$ that desorbs after the water ice mantle is 98.5% ± 0.5. This high yield shows that an important part of nitrogen is released after the water ice has completely desorbed.

(v) It is fundamental to consider the chemical nature of the N-bearing molecules to correctly model their desorption in astrophysical environments. As we have seen in this study, the ammonium sublimation zone turns out to be closer to the protostar with respect to the water snow-line. This has important implications with regard to the nitrogen reservoir available across the protoplanetary disk.

References

Acharyya, K., Fuchs, G. W., Fraser, H. J., van Dishoeck, E. F., & Linnartz, H. 2007, A&A, 466, 1005

Alexander, C., Cody, G., Gregorio], B. D., Nittler, L., & Stroud, R. 2017, Geochem., 77, 227

Alexander, C. M. O., Bowden, R., Fogel, M. L., et al. 2012, Science, 337, 721

Altwegg, K., Balsiger, H., Hänni, N., et al. 2020, Nat. Astron., 3

Bahr, S., Borodin, A., Höfft, O., Kempter, V., & Allouche, A. 2005, J. Chem. Phys., 122, 234704

Bahr, S., Borodin, A., Höfft, O., et al. 2006, J. Phys. Chem. B, 110, 8649, pMID: 16640419

Bergner, J. B., Öberg, K. I., Rajappan, M., & Fayolle, E. C. 2016, ApJ, 829, 85

Bertin, M., Martin, I., Duvernay, F., et al. 2009, Phys. Chem. Chem. Phys., 11, 1838

Bisschop, S. E., Fuchs, G. W., van Dishoeck, E. F., & Linnartz, H. 2007, A&A, 474, 1061

Bonal, L., Huss, G. R., Krot, A. N., et al. 2010, Geochim. Cosmochim. Acta, 74, 6590

Boogert, A. C. A., Gerakines, P. A., & Whittet, D. C. B. 2015, ARA&A, 53, 541

Bossa, J. B., Theulé, P., Duvernay, F., Borget, F., & Chiavassa, T. 2008, A&A, 492, 719

Bouilloud, M., Fray, N., Bénilan, Y., et al. 2015, MNRAS, 451, 2145

Burke, D. J., Puletti, F., Woods, P. M., et al. 2015, J. Phys. Chem. A, 119, 6837

Caffau, E., Maiorca, E., Bonifacio, P., et al. 2009, A&A, 498, 877

Caselli, P., Bizzocchi, L., Keto, E., et al. 2017, A&A, 603, L1

Caselli, P. & Ceccarelli, C. 2012, A&A Rev., 20, 56

Chaabouni, H., Baouche, S., Diana, S., & Minissale, M. 2020, A&A, 636, A4

Chaabouni, H., Diana, S., Nguyen, T., & Dulieu, F. 2018, A&A, 612, A47

Congiu, E., Sow, A., Nguyen, T., Baouche, S., & Dulieu, F. 2020, Rev. Sci. Inst., 91, 124504

D'Angelo, M., Cazaux, S., Kamp, I., Thi, W. F., & Woitke, P. 2019, A&A, 622, A208

D'Hendecourt, L. B. & Allamandola, L. J. 1986, A&AS, 64, 453

Faure, A., Faure, M., Theulé, P., Quirico, E., & Schmitt, B. 2015a, A&A, 584, A98

Faure, M., Quirico, E., Faure, A., et al. 2015b, Icarus, 261, 14

Filacchione, G., Groussin, O., Herny, C., et al. 2019, Space Sci. Rev., 215, 19

Fray, N., Bardyn, A., Cottin, H., et al. 2017, MNRAS, 469, S506

Gálvez, O., Maté, B., Herrero, V. J., & Escribano, R. 2010, ApJ, 724, 539

Grevesse, N., Asplund, M., Sauval, A. J., & Scott, P. 2010, Ap&SS, 328, 179

Góbi, S., Bergantini, A., Turner, A. M., & Kaiser, R. I. 2017, J. Phys. Chem. A, 121, 3879

Hellebust, S., O'Riordan, B., & Sodeau, J. 2007, J. Chem. Phys., 126, 084702

Hily-Blant, P., Bonal, L., Faure, A., & Quirico, E. 2013, Icarus, 223, 582

Hily-Blant, P., Walmsley, M., Pineau Des Forêts, G., & Flower, D. 2010, A&A, 513, A41

Ito, K. & Bernstein, H. J. 1956, Revue canadienne de chimie, 34, 170

Knauth, D. C., Andersson, B. G., McCandliss, S. R., & Warren Moos, H. 2004, Nature, 429, 636

Lodders, K. 2010, in Principles and Perspectives in Cosmochemistry, ed. A. Goswami & B. E. Reddy (Berlin, Heidelberg: Springer Berlin Heidelberg), 379–417

Lorin, A. & al. 1864, Chem. News and J. Phys. Sci., IX, 291

Maiolino, R. & Mannucci, F. 2019, A&A Rev., 27, 3

Maret, S., Bergin, E. A., & Lada, C. J. 2006, Nature, 442, 425

Martín-Doménech, R., Muñoz Caro, G. M., Bueno, J., & Goesmann, F. 2014, A&A, 564, A8

Marty, B. 2012, Earth Planet. Sci. Lett., 313, 56

Mispelaer, F., Theule, P., Duvernay, F., Roubin, P., & Chiavassa, T. 2012, A&A, 540, A40

Nieva, M. F. & Przybilla, N. 2012, A&A, 539, A143

Noble, J. A., Theule, P., Borget, F., et al. 2013, MNRAS, 428, 3262

Noble, J. A., Theule, P., Duvernay, F., et al. 2014, Phys. Chem. Chem. Phys., 16, 23604

Öberg, K. I., Boogert, A. C. A., Pontoppidan, K. M., et al. 2011, ApJ, 740, 109

Omont, A. 2007, Rep. Prog. Phys., 70, 1099

Poch, O., Istiqomah, I., Quirico, E., et al. 2020, Science, 367, aaw7462

Potapov, A., Jäger, C., & Henning, T. 2020, Phys. Rev. Lett., 124, 221103

Potapov, A., Theulé, P., Jäger, C., & Henning, T. 2019, ApJ, 878, L20

Punanova, A., Caselli, P., Pineda, J. E., et al. 2018, A&A, 617, A27

Raunier, S., Chiavassa, T., Duvernay, F., et al. 2004, A&A, 416, 165

Riaz, B., Thi, W. F., & Caselli, P. 2018, MNRAS, 481, 4662

Rousselot, P., Pirali, O., Jehin, E., et al. 2014, ApJ, 780, L17

Sandford, S. A. & Allamandola, L. J. 1993, ApJ, 417, 815

Savage, B. D. & Sembach, K. R. 1996, ARA&A, 34, 279

Shiozawa, Y., Koitaya, T., Mukai, K., Yoshimoto, S., & Yoshinobu, J. 2015, J. Chem. Phys., 143, 234707

Sivaraman, B., Nair, B. G., Lo, J. I., et al. 2013, ApJ, 778, 157

Tafalla, M., Santiago-García, J., Hacar, A., & Bachiller, R. 2010, A&A, 522, A91

Tait, S. L., Dohnálek, Z., Campbell, C. T., & Kay, B. D. 2005, J. Chem. Phys., 122, 164708

Theulé, P., Duvernay, F., Danger, G., et al. 2013, Adv. Space Res., 52, 1567

Ulbricht, H., Zacharia, R., Cindir, N., & Hertel, T. 2006, Carbon, 44, 2931

Vernazza, P., Castillo-Rogez, J., Beck, P., et al. 2017, AJ, 153, 72

Vila-Costas, M. B. & Edmunds, M. G. 1993, MNRAS, 265, 199

Visser, R., Bruderer, S., Cazzoletti, P., et al. 2018, A&A, 615, A75

Viti, S., Collings, M. P., Dever, J. W., McCoustra, M. R. S., & Williams, D. A. 2004, MNRAS, 354, 1141

Viti, S. & Williams, D. A. 1999, MNRAS, 305, 755

Walsh, C., Millar, T. J., Nomura, H., et al. 2014, A&A, 563, A33

Zhu, R. S., Wang, J. H., & Lin, M. C. 2007, J. Phys. Chem. C, 111, 13831